

Giant magnetic-field-induced strains in polycrystalline Ni-Mn-Ga foams

M. Chmielus^{1*}, X. X. Zhang^{2*}, C. Witherspoon¹, D. C. Dunand² and P. Müllner^{1†}

The magnetic shape-memory alloy Ni-Mn-Ga shows, in monocrystalline form, a reversible magnetic-field-induced strain (MFIS) up to 10%. This strain, which is produced by twin boundaries moving solely by internal stresses generated by magnetic anisotropy energy¹⁻⁴, can be used in actuators, sensors and energy-harvesting devices⁵⁻⁷. Compared with monocrystalline Ni-Mn-Ga, fine-grained Ni-Mn-Ga is much easier to process but shows near-zero MFIS because twin boundary motion is inhibited by constraints imposed by grain boundaries⁸⁻¹⁰. Recently, we showed that partial removal of these constraints, by introducing pores with sizes similar to grains, resulted in MFIS values of 0.12% in polycrystalline Ni-Mn-Ga foams¹¹, close to those of the best commercial magnetostrictive materials. Here, we demonstrate that introducing pores smaller than the grain size further reduces constraints and markedly increases MFIS to 2.0–8.7%. These strains, which remain stable over >200,000 cycles, are much larger than those of any polycrystalline, active material.

The very high MFIS (up to 10%) shown by bulk monocrystalline Ni-Mn-Ga alloys^{12,13} is a plastic strain produced by twin-boundary motion, which can be recovered by reverse twin motion through reorientation of the applied magnetic field and alternatively by mechanical compressive loading in a perpendicular direction. Fully recoverable MFIS over >10⁸ magneto-mechanical cycles (MMCs) was reported for monocrystalline bulk Ni-Mn-Ga (ref. 14), with high actuation speed in the kilohertz regime being limited by eddy currents and inertia¹⁵. The above properties make magnetic shape-memory alloys exceptionally well suited for applications such as fast actuators with a long stroke and high precision (for example, for engine valves and ultrafast high-precision scanners and printers).

A severe shortcoming of magnetic shape-memory alloys is that very large MFIS have, so far, been achieved only for single crystals. Owing to constraints imposed by grain boundaries, the MFIS is near zero in randomly textured, fine-grained, polycrystalline Ni-Mn-Ga (ref. 16). To reduce these constraints and increase MFIS, coarse-grained, highly textured, polycrystalline Ni-Mn-Ga was produced by directional solidification and annealing⁸⁻¹⁰. Although these materials did not deform directly when exposed to a magnetic field, they showed a MFIS recovery of 1% after mechanical training¹⁷, and a similar strain when magnetic actuation was combined with acoustic excitation¹⁸.

Introducing porosity in Ni-Mn-Ga is a different approach, which we recently demonstrated¹¹ for reducing constraints imposed by grain boundaries, while maintaining the ease of processing associated with casting polycrystalline Ni-Mn-Ga. With 76% open porosity, these Ni-Mn-Ga foams show MFISs as high as 0.12%, which are fully reversible over 30 million cycles¹¹. Beyond their uses as actuators and sensors, these open-porosity foams allow

fluid flow, making them potentially useful as micropumps (with the fluid being squeezed directly by the foam deformation) and magnetocaloric materials¹⁹ (where the high surface-to-volume ratio of the foam enhances heat exchanges through a fluid).

The architecture of these previous foams¹¹ may be described as a construct of struts linked together at nodes. Annealing ensured that a bamboo grain structure developed, with each strut containing a few (or even a single) large 'bamboo grains' spanning the full width of the struts. With this microstructure, each strut behaves like a single crystal with high MFIS. However, the struts are constrained by the nodes, which are polycrystalline and thus show near-zero MFIS. Here, we address this issue by introducing fine porosity within the nodes connecting the struts surrounding coarse pores. The present foams are produced by the same replication method, using sodium aluminate powders as temporary place holders, previously developed for foams with a large pore size¹¹. A bimodal pore size distribution is used here to allow for rapid and complete removal of the sodium aluminate, which would be very difficult to achieve with a monomodal fine porosity. Figure 1a shows a polished cross-section of the foam, with 62% porosity, illustrating the bimodal pore-size distribution. Figure 1b shows, at higher magnification, the twin structure made visible by polarized light: twins span fully across individual monocrystalline struts (further examples are given in Supplementary Fig. S1). Large pores make, by volume, most of the porosity in the foam and the corresponding nodes contain a multitude of smaller pores, which create a second population of much finer struts and nodes. Single grains contain multiple small pores and nodes, and twins spanning across entire large struts ensure the unhindered motion of twin boundaries. Supplementary Fig. S2 shows scanning electron micrographs of the bimodal pore structure in more detail.

Temperature-dependent measurement of magnetization with a vibrating sample magnetometer revealed the phase-transformation temperatures of the foam to be 30 and 43 °C for the austenite start and finish temperatures, 35 and 24 °C for the martensite start and finish temperatures and 88 °C for the Curie temperature (see Supplementary Fig. S3). Magnetization measurements during the thermo-magnetic training yielded a saturation magnetization at room temperature of 73 Am² kg⁻¹.

A first series of magneto-mechanical experiments was carried out at ~16 °C under a rotating magnetic field of 0.97 T (Fig. 2). In the martensite phase, the foam showed an initial MFIS of 2.1%. This is a factor of 20 larger than values previously obtained for a polycrystalline foam with monomodal, large pores¹¹. The MFIS increased over the next 2,000 MMC to ~3.4%, stabilizing at this value up to 15,000 MMC, decreasing steadily to 2.0% up to 75,000 MMC and remaining stable at this value up to 161,000 MMC. The foam was then removed from the sample

¹Department of Materials Science & Engineering, Boise State University, Boise, Idaho 83725, USA, ²Department of Materials Science & Engineering, Northwestern University, Evanston, Illinois 60208, USA. *Also at: G1-1, Helmholtz Centre Berlin for Materials and Energy, Glienicke Str. 100, 14109 Berlin, Germany (M.C.); Harbin Institute of Technology, West Dazhi Street No. 92, 150001, Harbin, P. R. China (X.X.Z.). †e-mail: petermullner@boisestate.edu.

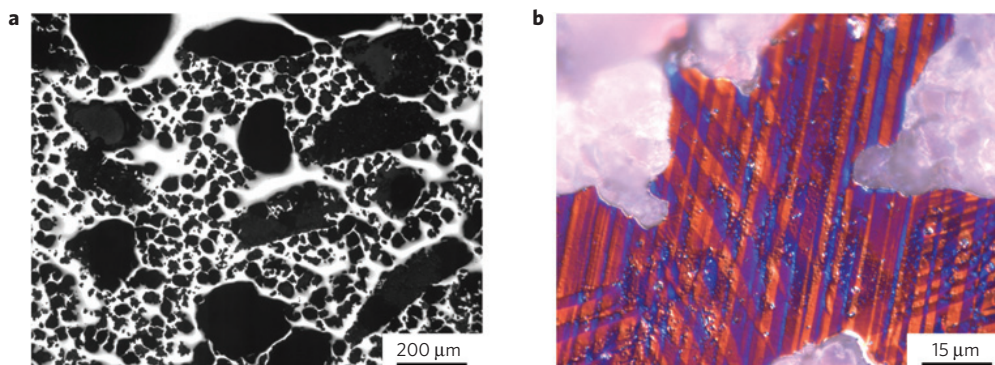


Figure 1 | Polished cross-section of Ni-Mn-Ga foam with a dual pore size. **a**, Optical micrograph at low magnification showing the small and large pores (black) within the Ni-Mn-Ga alloy (white). **b**, Optical micrograph of twins (coloured bands, made visible by cross-polarization), extending entirely from pore-to-pore (white).

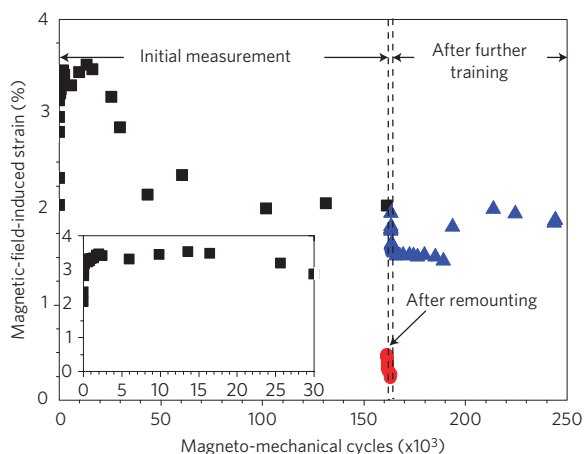


Figure 2 | Plot of MFIS versus magneto-mechanical cycles for the first series of tests at room temperature (~16 °C). The inset shows the first 30 cycles. After the initial test up to 161,000 cycles with MFIS of 2.0–3.6%, the foam was unmounted, inspected and remounted. The subsequent MFIS was low, so the foam was subjected to thermo-magnetic training before further magneto-mechanical testing with a MFIS of 1.4–2.1% up to 244,000 cycles.

holder for visual inspection and remounted after its integrity was confirmed. The subsequent MFIS was below 0.5%, probably because of misoriented twins introduced by handling during demounting and remounting. The foam was magnetically trained (see the Methods section) to eliminate these misoriented twins. The training was successful, as it re-established a high MFIS value that remained in the range 1.5–1.9% for a further 90,000 MMC.

A second series of magneto-mechanical experiments was carried out while the foam was thermally cycled between the martensite and austenite states, with the MFIS measured *in situ* in the rotating magnetic field. As shown in Fig. 3a, during the first heating through the phase transformation, the MFIS remains constant at 1.4% in the martensite phase before dropping rapidly to a near-zero value, over a temperature range of 35–41 °C corresponding to the end of the martensite–austenite transformation. The MFIS drop occurred over a finite temperature range, probably because of slight temperature gradients within the foam. On subsequent cooling, the MFIS increases sharply between 22 and 23 °C, very close to the M_f temperature, to a value of 2.2%. At the end of this first temperature cycle, the temperature was rapidly dropped to below –100 °C. At such low temperatures, Ni–Mn–Ga alloys undergo inter-martensitic transitions²⁰. As a result, on heating back to room temperature, the MFIS was strongly reduced to 0.2%. At the end

of the second temperature cycle, however, the MFIS recovered its original value of 2.5%. The MFIS further increased in the third and fourth temperature cycles, reaching an extraordinarily high value of 8.7% at the end of the fourth cycle, as shown in Fig. 3a. Supplementary Fig. S4a shows the MFIS magnitude as a function of the magnetic field orientation for a full field rotation before and after the first and second heating/cooling cycle and after the third and fourth heating/cooling cycle. A detailed view of the MFIS evolution on heating through the transformation temperature range during the third heating cycle is shown in Supplementary Fig. S4b, with the high MFIS value of 2.6% in the martensite at 29 °C decreasing steadily to near zero in the austenite at 35 °C. After the fourth heating/cooling cycle, the foam was unmounted, inspected and remounted. During the following six temperature cycles, the strain–temperature curves are very reproducible, with a MFIS after cooling of 4.4–5.1% (Fig. 3b).

The temperature hysteresis is slightly larger for the first four heating/cooling cycles (~15 K, see Fig. 3a) compared with the hysteresis for cycles 6–10 (~10 K, see Fig. 3b). Within each set of cycles, the hysteresis is however very consistent. The difference between the two sets is probably due to an experimental artefact of the temperature measurement. The thermocouple was placed loosely in a large pore and was not soldered to the foam to prevent heat effects and mechanical constraint. It is probable that the thermal contact was better in the second set of cycles, thus bringing the hysteresis closer to its true value. Owing to the better thermal contact, more details are resolved in the fifth–tenth temperature cycling curves (Fig. 3b), such as a shoulder in the strain–temperature cooling curve suggesting that the martensite transformation is discontinuous.

For the first four temperature cycles, the strain in the martensite phase just before the phase transformation on heating is significantly smaller than the strain just after the inverse transformation on cooling (Fig. 3c). The MFIS also increased from the fifth to the sixth cycle and then stabilized to a constant value of 4.4–5.1%, on either cooling or heating. These results can be explained by a training effect occurring during the first five thermo-magneto-mechanical cycling experiments. During cooling through the martensite transformation, the twin microstructure changes dynamically in response to the rotating magnetic field. Twins with an unfavourable orientation (that is, with their crystallographic c direction strongly misaligned with respect to the magnetic field direction) are steadily eliminated and replaced by twins with their c direction parallel to the direction of the magnetic field. After multiple austenite–martensite cycles, only highly mobile twins are left, which have their crystallographic c direction parallel to the plane in which the magnetic-field vector rotates, thus allowing for large MFIS.

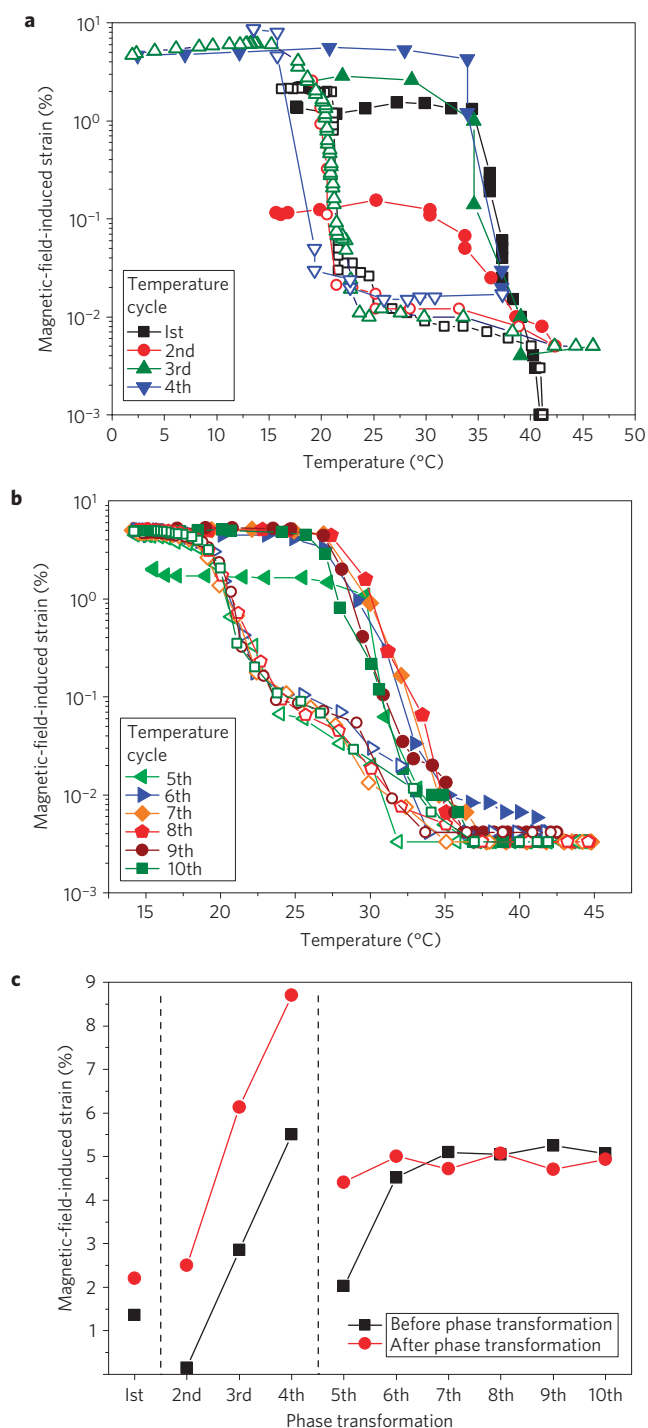


Figure 3 | MFIS measurement during the second series of tests, when the foam was thermally cycled ten times between its martensite and austenite phases. a, b, Plots of MFIS versus temperature for the thermal cycles 1–4 (a) and 5–10 (b), with filled symbols for heating and open symbols for cooling. **c,** Plot of the highest MFIS (just before and just after each phase transformation) versus cycle number. Supplementary Fig. S4a shows details for the first four cycles. The dashed vertical lines indicate unmounting and remounting of the foam during interruptions of the thermal cycling.

However, the elimination of poorly aligned twins by thermo-magneto-mechanical training cannot fully explain the extraordinary large MFIS values of 8.7% measured at the end of cycle 4. This is illustrated in Supplementary Fig. S5, which shows four

different alignments of austenite unit cells (top) (representing four grain orientations) and their matching martensite unit cells (bottom) with their c axes aligned to the magnetic field. The strain component in the z direction, which is measured during the present experiments, depends on the misalignment α of the c axis with respect to the z direction of the foam. Assuming a random texture, the average strain of each isolated, unconstrained monocrystalline strut is obtained from averaging $\cos\alpha$ between 0 and $\pi/4$ over the three Euler angles, which yields 73% of the single-crystal theoretical strain, which itself is given as $1 - c/a$ (where a and c are the martensite lattice parameters). Taking the value of $c/a = 0.90$ for a 14 M martensite, only 7.3% would be possible in a texture-free polycrystalline sample. The largest MFIS of 8.7% measured at the end of cycle 4 may indicate that the foam is textured, because of solidification or geometrical effects, such as plastic hinging of the struts due to a magnetic-field-induced torque, may be operative. Neutron diffraction experiments are planned in the near future to clarify these aspects.

For bulk Ni–Mn–Ga single crystals, it was shown¹⁴ that ineffectively trained samples can be magneto-mechanically trained in a setting where the sample is constrained. In this in-service training, the single crystal adopts a twin microstructure compatible with the applied constraints. Our results demonstrate that thermo-magneto-mechanical cycling is an effective in-service training for Ni–Mn–Ga foams that increases the MFIS even with constraints imposed by mounting the sample to a holder. This in-service training is more effective for the foam than for bulk single crystals¹⁴, a possible explanation being relaxation of external constraints. According to the St Venant principle, the stress field of a locally stressed material extends into the material to a distance that compares to the width of the loaded area. For a bulk sample, this stress-affected volume extends to about half the width of the glued (that is, constrained) face, which is about 1 mm. For a foam, the stress-affected zone may be significantly reduced and limited to a few strut diameters, which is of the order of 20 μm .

We have demonstrated that a polycrystalline Ni–Mn–Ga foam produced by a simple casting process shows very high MFIS values of 2.0–3.5%, as measured over 244,000 magneto-mechanical cycles. These values are three orders of magnitude larger than the MFIS of 0.002% (ref. 16) shown by non-porous, fine-grained Ni–Mn–Ga (and other magnetic shape-memory alloys) and 10–20 times larger than the strain produced by the best magnetostrictive materials, for example, commercial Terfenol-D with a strain of 0.2% (ref. 21). This marked improvement is attributed to a mechanical size effect, with the foam node size ($\sim 20 \mu\text{m}$) and strut width being smaller than the grain size, thus allowing the free motion of the twins responsible for the MFIS. Furthermore, the foam MFIS increased, on thermal cycling between the martensite and austenite phases, to an extraordinarily high value of 8.7%, similar to that of a well-oriented, bulk Ni–Mn–Ga single crystal. A stable value of 4.4–5.1% was reached after a few thermal cycles. These results open the door to the use of inexpensive, cast, polycrystalline Ni–Mn–Ga foams for long-stroke actuators with very rapid response rates and excellent stability over millions of cycles and for sensors, magnetic cooling systems and energy-harvesting devices^{5–7}.

Methods

The Ni–Mn–Ga foam was created by the replication method, which we developed earlier¹¹, using liquid metal infiltration of a preform of ceramic space-holder powders. Here, a 73:27 (by weight) blend of large (500–600 μm) and small (75–90 μm) sodium aluminate powders was used, unlike our previous publication¹¹ where only large powders were used. The blended powders were poured into an alumina crucible with a 9.7 mm diameter and lightly sintered in air at 1,500 °C for 3 h to create necks between powders. After cooling, two ingots of equal mass, with atomic compositions of $\text{Ni}_{52.0}\text{Mn}_{24.4}\text{Ga}_{23.6}$ and $\text{Ni}_{52.3}\text{Mn}_{23.9}\text{Ga}_{23.8}$, were placed on top of the sintered preform, which was then heated to 1,200 °C at 7 °C min^{-1} under a vacuum of 3.5×10^{-6} torr. High-purity argon gas was introduced in the furnace at a pressure of 1.34 atm to push the molten alloy into the preform

and the temperature was then dropped to room temperature at $7^{\circ}\text{C min}^{-1}$. The resulting Ni–Mn–Ga/sodium aluminate composite was cut with a diamond saw to create a parallelepiped sample with approximate dimensions of $x = 2.3$, $y = 3.0$ and $z = 6.2$ mm. Most of the sodium aluminate space holder was removed by immersion in 34% H_2SO_4 under ultrasonication. Immersion in 10% HCl removed the remaining sodium aluminate and thinned the foam struts, resulting in a porosity of 62%, as determined from measurements of mass and volume. The foam was homogenized at $1,000^{\circ}\text{C}$ for 1 h in vacuum and then subjected to a stepwise chemical ordering heat treatment (2 h at 725°C , 10 h at 700°C and 20 h at 500°C) to establish the L_{21} structure. The magnetic and thermal properties were measured using a Digital Measurement Systems Model 10 vibrating sample magnetometer with an applied magnetic field of 0.028 T parallel to the z direction: the foam was heated at 8.5 K min^{-1} to 150°C , and the temperature was held for 2 min and then reduced at 8.5 K min^{-1} to room temperature, where it was held for 5 min.

In a first series of magneto-mechanical experiments near ambient temperature ($\sim 16^{\circ}\text{C}$), the foam was exposed to a rotating magnetic field $\mu_0 H = 0.97\text{ T}$ while being glued at one end to a sample holder and at the other to a head capable of sliding only in the direction of the foam z axis (Supplementary Fig. S6). The magnetic-field rotational axis was parallel to the foam x axis (see Supplementary Fig. S6) with the magnetic-field vector rotating within the y – z plane. Although the steady-state rotation frequency of the magnetic field was 4,000 revolutions per minute (r.p.m.) for magneto-mechanical cycling, it was reduced to 30 r.p.m. during strain data acquisition to reduce noise. The foam minimum and maximum lengths were measured along the z axis (see Supplementary Fig. S4b) and transformed to MFIS values using the engineering definition of strain (ratio of maximum sample displacement to minimal sample length z). Further experimental details are given in ref. 12. At first, the foam was subjected to 80,000 field rotations, corresponding to 160,000 MMC (during one full rotation of the magnetic field, the foam contracts and expands twice, Supplementary Fig. S4b). The foam was then unmounted, inspected, remounted and magneto-mechanically tested for a further 2,000 MMC. The test was interrupted early because of low MFIS values. The foam was unmounted, thermo-magnetically trained by exposing it in the vibrating sample magnetometer to a magnetic field $\mu_0 H = 2\text{ T}$ parallel to the z direction while heating to, and then cooling from, 150°C with nitrogen at a rate of 8.5 K min^{-1} and remounted to the sample holder. Magneto-mechanical tests were then resumed under the same conditions as above for another 81,000 MMC.

A second series of magneto-mechanical experiments was carried out in the same apparatus while the temperature was cycled (as summarized in Supplementary Table S1) between ~ 15 and $\sim 40^{\circ}\text{C}$, encompassing the range of phase transformations. At the end of only the first cycle, the temperature was rapidly dropped to below -100°C . A thermocouple (marked (9) on Supplementary Fig. S6) was attached loosely to a pore at the top surface of the foam. Hot (for heating) and cold (for cooling) air was directed towards the sample chamber through a tube (5). Owing to the presence of a lid (8), the foam was protected from the direct air flow. Conduction through the sample holder and sliding head, as well as natural convection from the surrounding air were heating/cooling the foam indirectly and therefore smoothly. During the ten temperature cycles, the magnetic field was rotated at 30 r.p.m. allowing precise MFIS measurements, as shown in Supplementary Fig. S4c. The experiment was interrupted twice (before the second and the fifth cycles): the foam was then removed from the sample holder, inspected for damage and remounted.

Received 9 June 2009; accepted 3 August 2009; published online 13 September 2009

References

- Ullakko, K., Huang, J. K., Kantner, C., O'Handley, R. C. & Kokorin, V. V. Large magnetic-field-induced strains in Ni_2MnGa single crystals. *Appl. Phys. Lett.* **69**, 1966–1968 (1996).
- James, R. D. & Wuttig, M. Magnetostriction of martensite. *Phil. Mag.* **A 77**, 1273–1299 (1998).
- Murray, S. J. *et al.* Large field induced strain in single crystalline Ni–Mn–Ga ferromagnetic shape memory alloy. *J. Appl. Phys.* **87**, 5774–5776 (2000).
- Müllner, P., Chernenko, V. A., Wollgarten, M. & Kostorz, G. Large cyclic deformation of a Ni–Mn–Ga shape memory alloy induced by magnetic fields. *J. Appl. Phys.* **92**, 6708–6713 (2002).
- Suorsa, I., Tellinen, J., Ullakko, K. & Pagounis, E. Voltage generation induced by mechanical straining in magnetic shape memory materials. *J. Appl. Phys.* **95**, 8054–8058 (2004).

- Sarawate, N. & Dapino, M. Experimental characterization of the sensor effect in ferromagnetic shape memory Ni–Mn–Ga. *Appl. Phys. Lett.* **88**, 121923 (2006).
- Karaman, I., Basaran, B., Karaca, H. E., Karsilayan, A. I. & Chumlyakov, Y. I. Energy harvesting using martensite variant reorientation mechanism in a NiMnGa magnetic shape memory alloy. *Appl. Phys. Lett.* **90**, 172505 (2007).
- Galetzsch, U., Roth, S., Rellinghaus, B. & Schultz, L. Adjusting the crystal structure of NiMnGa shape memory ferromagnets. *J. Magn. Magn. Mater.* **305**, 275–277 (2006).
- Galetzsch, U., Pötschke, M., Roth, S., Rellinghaus, B. & Schultz, L. Mechanical training of polycrystalline $7\text{M Ni}_{50}\text{Mn}_{30}\text{Ga}_{20}$ magnetic shape memory alloy. *Scr. Mater.* **57**, 493–495 (2007).
- Pötschke, M., Galetzsch, U., Roth, S., Rellinghaus, B. & Schultz, L. Preparation of melt textured Ni–Mn–Ga. *J. Magn. Magn. Mater.* **316**, 383–385 (2007).
- Boonyongmaneerat, Y., Chmielus, M., Dunand, D. C. & Müllner, P. Increasing magnetoplasticity in polycrystalline Ni–Mn–Ga by reducing internal constraints through porosity. *Phys. Rev. Lett.* **99**, 247201 (2007).
- Müllner, P., Chernenko, V. A. & Kostorz, G. Large cyclic magnetic-field-induced deformation in orthorhombic (14M) Ni–Mn–Ga martensite. *J. Appl. Phys.* **95**, 1531–1536 (2004).
- Sozinov, A., Likhachev, A. A., Lanska, N. & Ullakko, K. Giant magnetic-field-induced strain in NiMnGa seven-layered martensitic phase. *Appl. Phys. Lett.* **80**, 1746–1746 (2002).
- Chmielus, M., Chernenko, V. A., Knowlton, W. B., Kostorz, G. & Müllner, P. Training, constraints, and high-cycle magneto-mechanical properties of Ni–Mn–Ga magnetic shape-memory alloys. *Eur. Phys. J. Special Topics* **158**, 79–85 (2008).
- Marioni, M. A., O'Handley, R. C. & Allen, S. M. Pulsed magnetic field-induced actuation of Ni–Mn–Ga single crystals. *Appl. Phys. Lett.* **83**, 3966–3968 (2003).
- Lázpita, P., Rojo, G., Gutiérrez, J., Barandiaran, J. M. & O'Handley, R. C. Correlation between magnetization and deformation in a NiMnGa shape memory alloy polycrystalline ribbon. *Sensor Lett.* **5**, 65–68 (2007).
- Galetzsch, U., Pötschke, M., Roth, S., Rellinghaus, B. & Schultz, L. A 1% magnetostrain in polycrystalline 5M Ni–Mn–Ga. *Acta Mater.* **57**, 365–370 (2009).
- Galetzsch, U., Techapiensancharoenkij, R., Pötschke, M., Roth, S. & Schultz, L. Acoustic assisted magnetic field induced strain in 5M Ni–Mn–Ga polycrystals. *IEEE Trans. Magn.* **45**, 1919–1921 (2009).
- Gschneidner, K. A. Jr & Pecharsky, V. K. Recent developments in magnetocaloric materials. *Rep. Prog. Phys.* **68**, 1479–1539 (2005).
- Segui, C. *et al.* Low temperature-induced intermartensitic phase transformations in Ni–Mn–Ga single crystals. *Acta Mater.* **53**, 111–120 (2005).
- Hathaway, K. & Clark, A. E. Magnetostrictive materials. *MRS Bull.* **18**, 34–41 (1993).

Acknowledgements

The authors thank A. Rothenbühler (Boise State University) for assistance with magnetic and magneto-mechanical experiments. This project was financially supported by the National Science Foundation through grant NSF-DMR 0804984 (Boise State University) and DMR-805064 (Northwestern University). M.C. acknowledges partial financial support through the German Research Foundation (DFG) priority program SPP 1239 (grant No. Schn 1106/1). P.M. is grateful to ETH Zürich for donating magneto-mechanical testing devices.

Author contributions

X.X.Z. produced the foam and characterized its architecture, twin microstructure and porosity. M.C. and C.W. carried out the magnetic and magneto-mechanical experiments. M.C. analysed the data and wrote the first version of the manuscript, with contributions from X.X.Z. P.M. and D.C.D. conceived the dual-porosity strategy, supervised the experiments at their respective universities and completed the manuscript.

Additional information

Supplementary information accompanies this paper on www.nature.com/naturematerials. Reprints and permissions information is available online at <http://npg.nature.com/reprintsandpermissions>. Correspondence and requests for materials should be addressed to P.M.